A Structural Basis for the Chiral Preferences of Lipases

Miroslaw Cygler,*,† Paweł Grochulski,†,‡ Romas J. Kazlauskas,*,§ Joseph D. Schrag,† François Bouthillier,† Byron Rubin,§,⊥ Alessio N. Serreqi,§ and Ajay K. Gupta§

Contribution from the Biotechnology Research Institute, National Research Council of Canada,‖ 6100 Royalmount Avenue, Montréal, Québec H4P 2R2, Canada, McGill University, Department of Chemistry, 801 Sherbrooke St. W., Montréal, Québec H3A 2K6, Canada, and Sterling Winthrop Inc., Sterling Winthrop Pharmaceuticals Research Division, Collegeville, Pennsylvania 19460

Received October 20, 1993®

Abstract: Many lipases and esterases show striking similarities in their enantioselectivities, and empirical rules have been formulated to predict the preferred stereochemistry for various types of reactions. A rule for formation of secondary alcohols predicts which enantiomer reacts faster based on the relative sizes of the substituents at the stereocenter. We report the first direct determination of the mechanism by which a lipase distinguishes between enantiomers and provide a general structural explanation of the aforementioned empirical rule. We determined X-ray crystal structures of covalent complexes of *Candida rugosa* lipase with transition-state analogs for the hydrolysis of menthyl esters. One structure contains (1*R*)-menthyl hexylphosphonate, **1*R***, derived from the fast-reacting enantiomer of menthol; the other contains (1S)-menthyl hexylphosphonate, **1*S***, derived from the slow-reacting enantiomer. These high-resolution three-dimensional structures show, firstly, that the empirical rule determined by substrate mapping is a good low-resolution description of the alcohol binding site in *Candida rugosa* lipase. Secondly, interactions between the menthyl ring of the slow-reacting enantiomer and the histidine of the catalytic triad disrupt the hydrogen bond between Nϵ2 of the imidazole ring and the menthol oxygen atom, likely accounting for the slower reaction of the (1*S*)-enantiomer of menthol. Thirdly, the enantiopreference of CRL toward secondary alcohols is set, not by an alcohol binding site separate from the catalytic site but by the same loops that assemble the catalytic machinery. The common orientation of these loops among many lipases and esterases accounts for their common enantiopreference toward secondary alcohols. This identification of the enantioselection mechanism sets the stage for rational enantioselective syntheses with lipases.

Introduction

For an enantioselective catalyst to be generally useful, it must combine two opposing qualities. It must accept a broad range of substrates, yet retain high enantioselectivity for each one. Lipases (triacylglycerol hydrolases) are among the few catalysts that fulfill both criteria, and for this reason organic chemists often use lipases for the synthesis of enantiomerically-pure compounds. These stable and inexpensive enzymes catalyze not only the hydrolysis of natural esters of glycerol and cholesterol but also hydrolysis and transesterification of a broad range of unnatural esters which serve as precursors to pharmaceuticals, agrochemicals, and other synthetic targets.[1] To identify why lipases retain high enantioselectivity over a broad range of substrates, chemists need to know the mechanism by which lipases distinguish between enantiomers.

Until now, the mechanism of enantiorecognition has been probed only by substrate mapping. The common structural features among well-resolved substrates have been summarized in empirical rules for enantiopreference. For example, based on the observed enantioselectivities of lipases toward hundreds of secondary alcohols for hydrolysis reactions, where the substrate is an ester, and for esterification reactions, where the substrate is an alcohol, an empirical rule was formulated. It predicts which enantiomer of a secondary alcohol reacts faster in lipase-catalyzed reactions by comparing the sizes of the substituents at the stereocenter. This rule is represented schematically in Figure 1. When the alcohol is drawn with the hydroxyl group pointing forward, out of the plane of the page, the favored enantiomer bears a large substituent on the right, e.g., phenyl, and a medium substituent on the left, e.g., methyl. The importance of substituent size was confirmed by studies which showed that lipases resolve secondary alcohols with two similarly-sized substituents poorly, but they resolve these secondary alcohols efficiently when the size of one substituent is increased.[2-4] Although the degree of enantioselectivity varies for different alcohols and enzymes, all

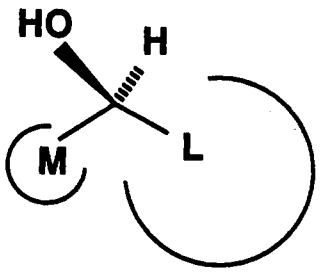

Figure 1. Enantiorecognition by CRL. Empirical rule that predicts which enantiomer of a secondary alcohol reacts faster with CRL and eleven other hydrolases. This schematic shows the favored enantiomer for secondary alcohols. The hydroxyl group points forward out the plane of the page; M represents a medium substituent, e.g., $-CH_2CH(CH_3)-$; L represents a large substituent, e.g., $-CH[CH(CH_3)_2]CH_2-$. This rule generalizes the observed enantioselectivity of hydrolases of both hydrolysis reactions and transesterifications. In hydrolysis reactions, the substrate is the ester of the alcohol shown; in transesterification reactions, the substrate is an alcohol.

* Author to whom the correspondence should be addressed.
† Biotechnology Research Institute.
‡ Permanent address: Institute of Physics, Technical University of Łódź, 93-005 Łódź, Poland.
‖ McGill University.
⊥ Sterling Winthrop Inc.
‖ NRCC publication No. 36164.
® Abstract published in *Advance ACS Abstracts*, March 15, 1994.

(1) Reviews: (a) Sih, C. J.; Wu, S. H. *Top. Stereochem.* **1989**, *19*, 63–125. (b) Crout, D. H. G.; Christen, M. In *Modern Synthetic Methods*; Scheffold, R., Ed.; Springer-Verlag: Berlin, 1989; Vol. 5, pp 1–114. (c) Santaniello, E.; Ferraboschi, P.; Grisenti, P.; Manzocchi, A. *Chem. Rev.* **1992**, *92*, 1071–1140.

(2) Kazlauskas, R. J.; Weissfloch, A. N. E.; Rappaport, A. T.; Cuccia, L. A. *J. Org. Chem.* **1991**, *56*, 2656–2665.

0002-7863/94/1516-3180$04.50/0

Scheme 1

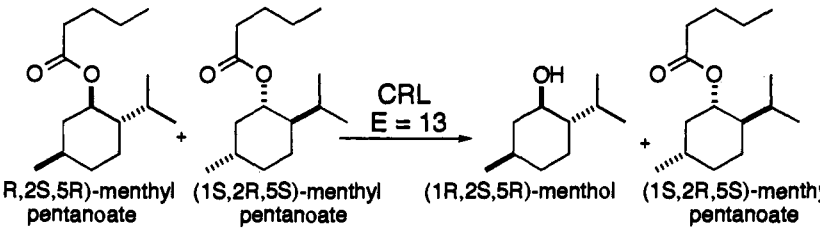

lipases and esterases prefer the enantiomer shown. This empirical rule helps organic chemists predict the favored enantiomer in new lipase-catalyzed reactions and provides a strategy to increase the enantioselectivity of these reactions, but neither identifies the detailed mechanism of enantiorecognition nor explains how lipases maintain high enantioselectivity for such a wide range of substrates.

From the substrate mapping, researchers concluded that lipases and esterases probably use a similar mechanism for enantiorecognition because they all follow the same empirical rule. This mechanism probably involves structural features common to all lipases and esterases. Over the past three years, the high-resolution X-ray crystal structures of seven hydrolases have been reported. These include five lipases: *Rhizomucor miehei* lipase,[5] human pancreatic lipase,[6] *Geotrichum candidum* lipase,[7] *Candida rugosa* lipase,[8] and *Pseudomonas glumae* lipase,[9] as well as cutinase[10] and acetylcholinesterase.[11] These structures answered the question of what causes the increase in activity of lipases at hydrophobic surfaces. In solution a lid, or flap, covers the active site of the lipase, but in the presence of lipid or organic solvent, this flap moves away, thereby exposing the active site and increasing the rate of hydrolysis. The crystal structures also revealed that the three-dimensional structures of hydrolases are more similar than expected from the amino acid sequences. These seven hydrolases differ widely in size, ranging from 22 kD for cutinase to 60 kD for *Geotrichum candidum* lipase, and the only sequence motif common to all of them is a pentapeptide -Gly-X-Ser-X-Gly- which encompasses the active site serine. Nevertheless, all are serine esterases with a common arrangement of catalytic machinery and a protein chain that folds, at least in part, in an α/β hydrolase fold.[12] The α/β hydrolase fold contains a mostly parallel β-sheet in the core with α-helices surrounding this core. This folding pattern arranges the residues of the catalytic triad—Ser, His, and either Glu or Asp—in an identical manner in all these enzymes. The nucleophilic serine rests at a hairpin turn between a β-strand and an α-helix, the remaining two residues of the catalytic triad—His and either Asp or Glu—rest on one side of the serine, while the residues forming the oxyanion hole lie on the other.

To identify which of the common structural features in lipases are involved in enantiorecognition, we investigated by X-ray crystallography how lipase from *Candida rugosa* distinguishes between enantiomers of menthol. To mimic the transition state for hydrolysis of menthyl esters, we used phosphonates covalently linked to the active site serine. The three-dimensional structures of these complexes provide a detailed picture of the structural basis of enantioselection of secondary alcohols.

Results

Lipase from *Candida rugosa* (CRL) catalyzed the hydrolysis of (±)-menthyl pentanoate and favored the (1*R*)-enantiomer, Scheme 1. This enantiopreference, where the large substituent is -CH[CH(CH_3)$_2$]CH_2- and the medium substituent is -CH_2CH-(CH_3)-, agrees with the empirical rule depicted in Figure 1. The enantiomeric ratio (*E*),[13] which measures the enantioselectivity of the reaction, was 13, a value similar to that reported by others for various menthol esters.[14] CRL-catalyzed esterifications and transesterifications of menthol in organic solvents showed somewhat higher enantioselectivity.[14]

The reaction mechanism for hydrolysis of an ester catalyzed by a serine esterase, Scheme 2, shows that the enzyme releases the alcohol as the first tetrahedral intermediate collapses. Thus, the transition state that determines the enantioselectivity of the enzyme toward alcohols occurs during formation or collapse of this first tetrahedral intermediate, whichever step is slower. To mimic this transition state for the hydrolysis of menthyl heptanoate, we used a phosphonate covalently linked to the active site serine. The *O*-(1*R*,2*S*,5*R*)-menthyl hexylphosphonate group, **1*R***, mimics the transition state for the fast-reacting enantiomer, while the *O*-(1*S*,2*R*,5*S*)-menthyl hexylphosphonate group, **1*S***, mimics the transition state for the slow-reacting enantiomer.

We used the chloride derivatives, **1*R*-Cl** and **1*S*-Cl**, to link **1*R*** and **1*S*** to the active site serine of CRL, Ser 209, thereby inactivating the enzyme. Inactivator **1*R*-Cl** was prepared by the tetrazole-catalyzed reaction of hexylphosphonic dichloride[15] with (1*R*,2*S*,5*R*)-(-)-menthol in the presence of diisopropylethylamine. This reaction replaced one chlorine and gave a 1:1 mixture of diastereomers (S_p)-**1*R*-Cl** and (R_p)-**1*S*-Cl**. Inactivator **1*S*-Cl** was prepared in a similar manner from (1*S*,2*R*,5*S*)-(+)-menthol. Addition of a 100-fold molar excess of either (S_p,R_p)-**1*R*-Cl** or (S_p,R_p)-**1*S*-Cl** to an aqueous solution of CRL irreversibly eliminated the ability of CRL to catalyze the hydrolysis of *p*-nitrophenyl acetate; activity dropped to <2% of the original value.

This inactivated enzyme crystallized under the same conditions as the open form of the unliganded enzyme[8] and yielded isomorphous crystals. We collected diffraction data as summarized in Table 1 and solved the three-dimensional structure using

(3) Kim, M. J.; Choi, Y. K. J. *Org. Chem.* **1992**, *57*, 1605–1607.
(4) Georgens, U.; Schneider, M. P. *J. Chem. Soc., Chem. Commun.* **1991**, 1066–1068.
(5) (a) Brady, L.; Brzozowski, A. M.; Derewenda, Z. S.; Dodson, E.; Dodson, G.; Tolley, S.; Turkenburg, J. P.; Christiansen, L.; Huge-Jensen, B.; Norskov, L.; Thim, L.; Menge, U. *Nature* **1990**, *343*, 767–770. (b) Brzozowski, A. M.; Derewenda, U.; Derewenda, Z. S.; Dodson, G. G.; Lawson, D.; Turkenburg, J. P. *Nature* **1991**, *351*, 491–494.
(6) (a) Winkler, F. K.; D'Arcy, A.; Humziker, W. *Nature* **1990**, *343*, 771–774. (b) van Tilbeurgh, H.; Sarda, L.; Verger, R.; Cambillau, C. *Nature* **1992**, *359*, 159–162. (c) van Tilbeurgh, H.; Egloff, M.-P.; Martinez, C.; Rugani, N.; Verger, R.; Carnbillau, C. *Nature* **1993**, *362*, 814–820.
(7) Schrag, J. D.; Li, Y.; Wu, S.; Cygler, M. *Nature* **1991**, *351*, 761–764. Schrag, J. D.; Cygler, M. *J. Mol. Biol.* **1993**, *230*, 575–591.
(8) Grochulski, P.; Li, Y.; Schrag, J. D.; Bouthillier, F.; Smith, P.; Harrison, D.; Rubin, B.; Cygler, M. *J. Biol. Chem.* **1993**, *268*, 12843–12847. For closed form see: Grochulski, P.; Li, Y.; Schrag, J. D.; Cygler, M. *Protein Science* **1994**, *3*, 82–91.
(9) Noble, M. E. M.; Cleasby, A.; Johnson, L. N.; Egmond, M. R.; Frenken, L. G. J. *FEBS Lett.* **1993**, *331*, 123–128.
(10) Martinez, C.; DeGeus, P.; Lauwereys, M.; Matthyssens, G.; Cambillau, C. *Nature* **1992**, *354*, 615–618.
(11) Sussman, J. L.; Harel, M.; Frolow, F.; Oefner, C.; Goldman, A.; Toker, L.; Silman, I. *Science* **1991**, *253*, 872–879.
(12) Ollis, D. L.; Cheah, E.; Cygler, M.; Dijkstra, B.; Frolow, F.; Franken, S. M.; Harel, M.; Remington, S. J.; Silman, I.; Schrag, J.; Sussman, J. L.; Verschueren, K. H. G.; Goldman, A. *Protein Eng.* **1992**, *5*, 197–211.
(13) Chen, C. S.; Fujimoto, Y.; Girdaukas, G.; Sih, C. J. *J. Am. Chem. Soc.* **1982**, *104*, 7294–7299.
(14) Yamaguchi, Y.; Komatsu, A.; Moroe, T. *J. Agric. Chem. Soc. Jpn.* **1976**, *50*, 619–620. Koshiro, S.; Sonomoto, K.; Tanaka, A.; Fukui, S. *J. Biotechnol.* **1985**, *2*, 47–57. Langrand, G.; Secchi, M.; Buono, G.; Baratti, J.; Triantaphylides, C. *Tetrahedron Lett.* **1985**, *26*, 1857–1860. Langrand, G.; Secchi, M.; Buono, G.; Triantaphylides, C. *Tetrahedron Lett.* **1986**, *27*, 29–32. Lokotsch, W.; Fritsche, K.; Syldatk, C. *Appl. Microbiol. Biotechnol.* **1989**, *31*, 467–472. Rabiller, C. G.; Königsberger, K.; Faber, K.; Griengl, H. *Tetrahedron* **1990**, *46*, 4231–4240.
(15) Zhao, K.; Landry, D. W. *Tetrahedron* **1993**, *49*, 353–368.

Scheme 2

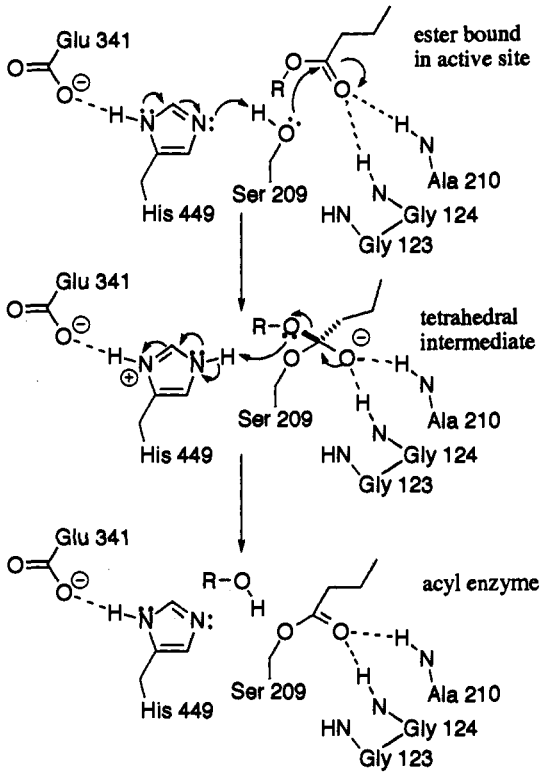

Table 1. Summary of the Crystallographic Analyses

	CRL-1*R*	CRL-1*S*
inhibitor–lipase ratio	30:1	65:1
resolution range (Å)	8–2.2	8–2.2
space group	$C222_1$	$C222_1$
unit cell dimensions		
a (Å)	65.2	65.1
b (Å)	97.5	97.7
c (Å)	176.3	176.1
total no. of observations	68189	66483
R merge (%)	10.7	8.1
completeness of the data (%)	84.8	80.4
no. of unique reflcns	24584	23157
with $I \geq 2\sigma(I)$	19378	18430
no. of solvent molecules		
H_2O	261	156
Ca^{2+}	2	2
no. of sugar molecules	3	3
final *R* factor		
for $I \geq 2\sigma(I)$	0.136	0.137
for all data	0.165	0.162
rms deviations from ideality for		
bond lengths (Å)	0.014	0.013
bond angles (deg)	2.74	2.71
av *B* factor (Å^2)	20.0	16.5

initial phases calculated from the open form of CRL.[8] The structures of the CRL–menthyl phosphonate complexes show no significant differences from the unliganded open conformation in the polypeptide backbone.

Both phosphonate groups bind similarly and in a manner consistent with their role as transition-state analogs. Both link covalently to Oγ of Ser 209 and have S_p stereochemistry at phosphorus. Since nucleophilic displacements at phosphorus occur with inversion in similar phosphonates,[16] the S_p stereochemistry indicates that only the (S_p)-**1*R*-Cl** and (S_p)-**1*S*-Cl** diastereomers in the original mixture of (S_p,R_p)-diastereomers reacted, Scheme 3. Note that, in spite of the inversion of configuration, the priority rules yield the S_p designation for both the starting phosphonyl chloride and the inverted product phosphonate. The phosphonyl oxygens of both **1*R*** and **1*S*** rest in the oxyanion hole within hydrogen-bonding distance of the amide NH groups of Ala 210 and Gly 124. In other CRL–inhibitor complexes the amide NH of Gly 123 also hydrogen bonds to the oxyanion.[17] In the **1*R*** and **1*S*** complexes the amide NH of Gly 123 is within hydrogen bonding distance of the phosphonyl oxygen, but the electron density suggests that the amide is directed toward a water molecule opposite the phosphonyl oxygen, making the geometry of a potential Gly 123 to phosphonyl oxygen hydrogen bond less than ideal. The contribution of the amide NH of Gly 123 to oxyanion stabilization is, thus, secondary to the contributions of Gly 124 and Ala 210. The hexyl chain binds in a tunnel that extends toward the center of the enzyme, while the menthyl rings lie at the entrance to the tunnel in a crevice open to the solvent.

The model of the alcohol-binding site generalized from the empirical rule for secondary alcohols (Figure 1) is consistent with the overall shape of the binding crevice observed in the crystal structures. This crevice has an oval shape with approximate dimensions 7 Å × 12 Å, in agreement with a previous estimate by substrate mapping,[18] and is positioned on the C-terminal ends of the β-strands (Figure 2). The large substituent -CH[CH-$(CH_3)_2$]CH_2- points into a hydrophobic region that is lined with phenyl rings (Figure 2a) and is open to the solvent, while the medium substituent -$CH_2CH(CH_3)$- rests on the floor of the crevice.

The amino acid residues from the catalytic machinery and from the loops that hold the catalytic machinery in place determine the shape of this alcohol-binding crevice (Figures 2b and 3). Two amino acid residues form the floor of the crevice directly below the menthol ring: Glu 208 and Gly 122. Glu 208 comes from the strand that holds Ser 209 in place, while Gly 122 forms part of the oxyanion-stabilizing loop (residues 122–125). In addition, two more residues form the floor further away from the menthol ring: Ile 453 and Phe 133. Three residues form the wall of the crevice on the side of the oxyanion hole: Gly 123, Gly 124, and Phe 296. As described above, Gly 124 and possibly Gly 123 are oxyanion stabilizing residues. His 449 from the catalytic triad and Ser 450 from the loop that holds His 449 in place form the other wall of the crevice. Thus, amino acid residues that are essential to catalysis also form the alcohol binding site.

While the menthyl rings of **1*R*** and **1*S*** both adopt similar edge-on orientations which point the isopropyl substituent upward, the opposite absolute configurations of the two menthyl moieties cause different interactions with the amino acid side chains in the crevice. The isopropyl substituent in **1*R*** is directed toward the side chains of Ile 297 and Phe 296 (Figure 3). In addition, Phe 344 and Phe 345 contribute also to the binding site for the isopropyl substituent. Compared to the unliganded open structure of CRL, the ring of Phe 344 became ordered, the side chain of Ile 297 adjusted slightly, and the ring of Phe 296 moved by approximately 1 Å to create more space for the isopropyl group. In contrast, the isopropyl group of **1*S*** is directed toward Phe 344 (Figure 3) and pushes against the rings of Phe 345 and His 449, both of which rotated by ~60°. As in the **1*R***–CRL complex, the side chain of Phe 344 becomes ordered and there is a small movement of the ring of Phe 296 toward the cyclohexyl ring. These adjustments for the isopropyl substituents in the two structures suggest that the side chains in this large hydrophobic pocket are flexible and can adjust to accommodate different substrates.

The most significant difference between the two complexes is the orientation of the imidazole ring of His 449 from the catalytic triad, Figures 3 and 4. In **1*R***–CRL the imidazole orients as in the unliganded open form of CRL[8] and Nε2 of His 449 forms a

(16) Corriu, R. J. P.; Lanneau, G. F.; Leclercq, D. *Tetrahedron* **1980**, *36*, 1617–1626.

(17) Grochulski, P.; Bouthillier, F.; Kazlauskas, R. J.; Serreqi, A. N.; Schrag, J. D.; Ziomek, E.; Cygler, M. *Biochemistry* **1994**, in press.

(18) Exl, C.; Hönig, H.; Renner, G.; Rogl-Kohlenprath, R.; Seebauer, V.; Seufer-Wasserthal, P. *Tetrahedron: Asymmetry* **1992**, *3*, 1391–1394.

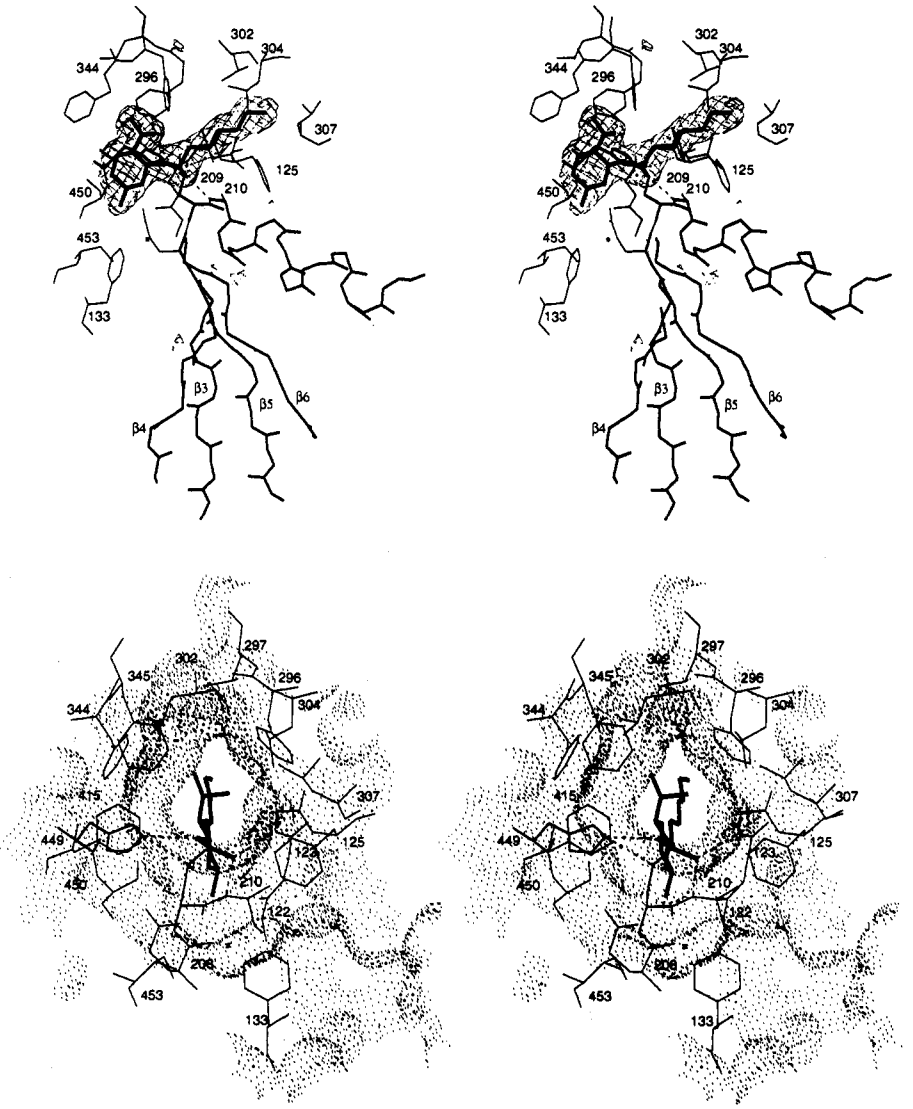

Figure 2. Stereodiagrams of structures of CRL–**1*R*** determined by X-ray crystallography. (a, top) Orientation of **1*R*** relative to the conserved elements of the α/β hydrolase fold (medium lines). The difference density ($F_o - F_c$) shown was calculated omitting the inhibitor from the model and is contoured at 2.5σ. The model of **1*R*** is shown in thick lines. The inhibitor links covalently to Ser 209, which lies at a sharp turn between strand β5 and an α helix. The remainder of the protein extends to the right and the solvent approaches from the left. (b, bottom) A different view of CRL–**1*R***. Dots represent the molecular surface[46] near the active site. The cyclohexyl ring lies parallel to the β-strands and the isopropyl substituent binds in a hydrophobic pocket at the top of the crevice. Dashed lines show the hydrogen bonds between the phosphonyl oxygen and NH of Ala 210 and Gly 124 and a bifurcated hydrogen bond between Nϵ2 of His 449 and Oγ of Ser 209 and O_1 of the menthyl moiety.

Scheme 3

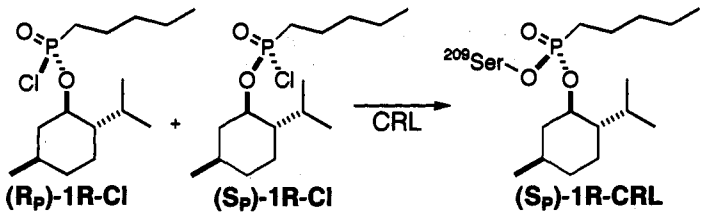

bifurcated hydrogen bond to Oγ of Ser 209 and to O1 of menthol. This bifurcated hydrogen bond is consistent with the proposed role of the imidazole ring in the catalytic mechanism, Scheme 2. The imidazole removes a proton from Oγ of Ser 209 to increase its nucleophilicity during the formation of the first tetrahedral intermediate and adds the proton to the oxygen of the alcohol to make it a better leaving group during the collapse of this tetrahedral intermediate. In contrast, when **1*S*** binds to CRL, the imidazole ring of His 449 rotates by ~60° and breaks the hydrogen bond between Nϵ2 of the imidazole ring and O1 of the menthol.

The mean planes of both cyclohexyl rings are nearly parallel to the strands of the β-sheet in the core and the edges of the rings with the methyl substituents rest on the crevice floor. To adopt this similar orientation with menthyl rings of opposite configuration requires different torsion angles along the P–O1 and O1–C1 bonds in the two structures, Figure 4. The Oγ–P–O1–C1 torsion angle is 138° in **1*R*** and 66° in **1*S***; the P–O1–C1–O2 torsion angles are 147° in **1*R*** and 162° in **1*S***. These differences alone place O1 ~0.3 Å farther from the native conformation of His 449 in **1*S*** than in **1*R***. Thus, the origin of the broken hydrogen bond is (1) the turning of the imidazole of His 449 caused by the

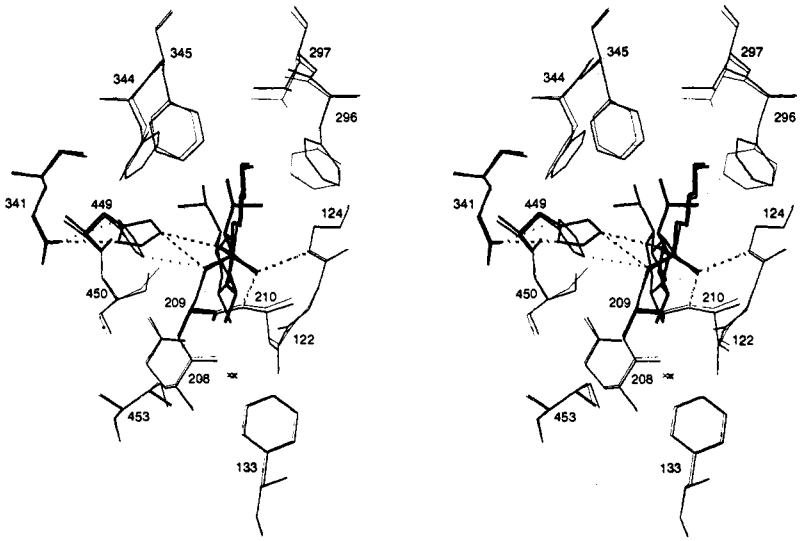

Figure 3. Superposition of CRL–1*R* (thick lines) and CRL–1*S* (thin lines) complexes. Both rings bind in similar orientations in the center of the crevice. The methyl substituent fills a small depression in the crevice floor. The hydrogen bond between Nε2 of His 449 and O1 of the menthyl moiety is absent.

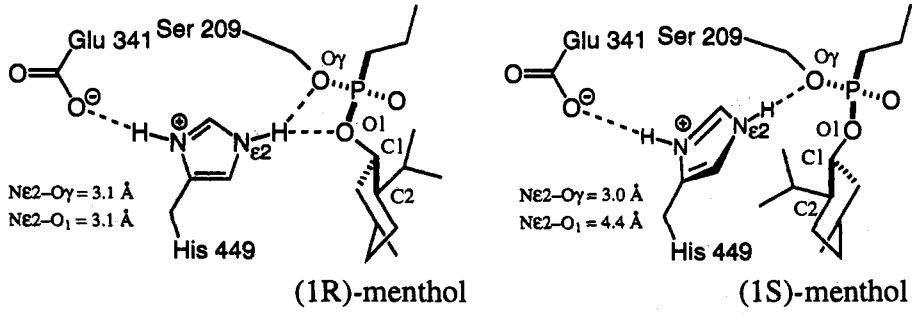

Figure 4. Schematic diagram of the hydrogen bonds between inactivators 1*R* and 1*S* and the imidazole of the catalytic triad. The isopropyl substituent of 1*R* points away from His 449. Both Oγ of Ser 209 and O1 of the menthol lie within the hydrogen-bonding distance of Nε2 of His 449: 3.09 and 3.14 Å, respectively. On the other hand, the isopropyl substituent of 1*S* points toward the imidazole ring of His 449. This imidazole ring turns by ~60° as compared to either the structure containing bound 1*R* or the unliganded structure. The Nε2 still lines within the hydrogen-bonding distance of Oγ of Ser 209, 3.00 Å, but O1 of menthol lies too far from Nε2 to form a hydrogen bond, 4.36 Å. We propose that this lack of a hydrogen bond between Nε2 and O1 of (1*S*)-menthol accounts for the slower reactivity of (1*S*)-menthyl esters. The proposed mechanism requires protonation of O1 of menthol during collapse of the tetrahedral intermediate. The lack of a hydrogen bond between Nε2 and O1 of (1*S*)-menthol suggests that this collapse may be slower than for (1*R*)-menthol.

isopropyl substituent and (2) the shift of the alcohol oxygen away from His 449 because of the opposite configuration at the carbinol stereocenter. We propose that disruption of this hydrogen bond in the 1*S*–CRL structure accounts for the slower reaction of this enantiomer.

To confirm that the lack of this hydrogen bond in the 1*S* structure can account for the differences in reactivity, we used molecular mechanics calculations. While allowing 1*S* and all the amino acid residues within 5.0 Å to freely adjust, we calculated a cost of 0.9 kcal/mol (CVFF force field) for moving the imidazole ring to within the hydrogen-bonding distance of O1. This value agrees well with the measured difference of 1.5 kcal/mol (E = 13) for the enantiomers of menthyl pentanoate. The different conformations of 1*R* and 1*S* observed in the enzyme both represent similar energy minima in the absence of enzyme. Minimization with the Chem 3D force field starting from the conformations determined by X-ray crystallography led to only small adjustments and similar potential energies: 1*R*, 13.9 kcal/mol; 1*S*, 13.4 kcal/mol. Replacement of phosphorus by carbon also gave even more equal energies for the two conformations: 34.3 and 34.2 kcal/mol. These calculations suggest that (1*R*,2*S*,5*R*)-menthyl pentanoate reacts faster than its enantiomer, not due to different energies of the tetrahedral intermediates, but due to different interaction energies between the tetrahedral intermediates and CRL, specifically, the lack of a hydrogen bond between His 449 and O1 in the 1*S* structure.

Discussion

Although lipases are widely used as enantioselective catalysts by organic chemists, the structural basis for this enantioselectivity was unknown. The transition state analogs of *Candida rugosa* lipase (CRL) described in this paper show, for the first time, how the binding by a lipase of two enantiomers of a secondary alcohol differs. Upon binding of the slow reacting enantiomer, the steric requirements of the large substituent of the alcohol force a rotation of the imidazole ring of His 449, disrupting the hydrogen bond to the alcohol oxygen. The loss of this hydrogen bond is likely the cause of the differences in reactivity of the two enantiomers.

The empirical rule for CRL, which is a good description of the binding site observed by X-ray crystallography, has also been proposed for reactions of secondary alcohols catalyzed by other enzymes, including lipases from *Pseudomonas sp.* (Amano lipase AK[19] or YS[20]), *P. cepacia* (Amano P or PS),[2,21,22] *P. aeruginosa*,[23] *P. fluorescens* (SAM-2),[24] *Rhizomucor miehei*,[25] *Arthrobacter*

(19) Burgess, K.; Jennings, L. D. *J. Am. Chem. Soc.* **1991**, *113*, 6129–6139.
(20) Naemura, K.; Ida, H.; Fukuda, R. *Bull. Chem. Soc. Jpn.* **1993**, *66*, 573–577.
(21) Xie, Z.-F.; Suemune, H.; Sakai, K. *Tetrahedron: Asymmetry* **1990**, *1*, 395–402.
(22) Kim, M. J.; Choi, Y. K. *J. Org. Chem.* **1992**, *57*, 1605–1607.
(23) Kim, M. J.; Cho, H. *J. Chem. Soc., Chem. Commun.* **1992**, *19*, 1411–1413.
(24) Laumen, K. Ph.D. Thesis, BUGH-Wuppertal, 1987.
(25) Roberts, S. M. *Phil. Trans. R. Soc. London B* **1989**, *324*, 577–587.

sp.,[26] porcine pancreas,[27] pancreatic cholesterol esterase,[2] *Mucor* esterase,[27] cultures of *Rhizopus nigricans*,[28] and cultures of *B. subtilus* var. *Niger*.[29] As for CRL, these rules are generalizations based on the observed enantiopreference of these enzymes toward secondary alcohols. In all 12 cases the enantiomer preferred was that shown in Figure 1. Further support for the notion of common enantiopreference toward secondary alcohols comes from a survey of the enantiopreferences of hydrolases toward (±)-menthol. All commercial lipases tested,[30] including that from wheat germ, *Rhizopus sp.*, *Aspergillus niger*, *Geotrichum candidum*,[31] and *Penicillium simplicissimum*,[32] favor the (1*R*)-enantiomer. Pig liver esterase[33] and esterase from *Bacillus subtilis*[34] and cultures of many bacteria, yeasts, and fungi including *Ochrobactrum*,[35] *Rhodotorula mucilaginosa*,[36] *Gloeophyllum sepiarium*, and *Schizophyllum*[37] also favor hydrolysis of the (1*R*)-menthol esters. This consistent preference for the (1*R*)-enantiomer over such a wide range of enzymes and sources supports the notion that features common to all these enzymes must be responsible for this enantiopreference.

All of these lipases and esterases are likely to have a similar architecture of their catalytic triads and alcohol binding sites. As mentioned in the introduction, the known structures of lipases and esterases show a common arrangement of their catalytic machinery at the C-terminal ends of the conserved β-strands and the catalytic triad of CRL is typical of all of these enzymes. Pancreatic lipases share the same fold as the other lipases, although they differ in the topological location of the acid member of the catalytic triad. Nonetheless, the loop which corresponds to the triad acid-containing loop in the other lipases is present in pancreatic lipases as well.[38] Many other lipases and esterases for which the three-dimensional structures have not yet been determined show significant sequence similarities to one of the lipases whose structure is known, supporting the notion that all of their structures are similar. For example, *Rhizopus* and *Penicillium* lipase sequences[39] are very similar to the *Rhizomucor miehei* lipase (known three-dimensional structure[5]); pancreatic cholesterol esterase and *Geotrichum candidum* lipase are close relatives of CRL;[7,40] *Pseudomonas* lipases all have similar sequences[41] and the structure of one of these lipases was recently reported;[9] porcine pancreatic lipase has a sequence that is very similar to human pancreatic lipase, whose structure is known.[6]

To summarize, the common features of the catalytic machinery are the following: the serine is embedded in a tight turn at the top of the β-sheet between a β-strand and an α-helix; the triad histidine is positioned similarly by loops on one side of the serine and the oxyanion hole is formed on the other side. Similar structural features are displayed by acetylcholinesterase[11] and are likely common to a large family of homologous esterases.[40] The common positioning of the essential elements of the catalytic machinery at the top of the conserved β-sheet framework by these loops leads to similarities among lipases and esterases in the orientations of the substrate in the active site.[17] Our results indicate that these same loops form the binding site for and restrict the positions and orientations available to the leaving alcohol group. The greatest restrictions result from limited space around the catalytic residues on one side, the oxyanion hole on the other side, and the supporting β-sheet. The similar spatial arrangement of these essential elements observed in various lipases and predicted for many esterases explains the common enantiopreference of lipases and esterases for secondary alcohols. The side chains of the residues within these loops can alter the details of the binding pocket, influencing the enantiomeric ratio and giving lipases their individuality, but do not change the enantiopreference. The observed small adjustments of the positions of the side chains in the hydrophobic pocket suggest that this region can adjust to accommodate different substrates. This plasticity may explain how lipases retain high enantioselectivity toward such a broad range of substrates.

The empirical rules developed over the years have provided useful low-resolution models of the substrate binding sites of lipases and esterases. The high-resolution structures now available for some of these enzymes provide an opportunity to combine the knowledge of the enzyme's architecture with the chemists' vast observations of their function. This study is a step in that direction and modeling of interactions with other substrates will refine our understanding of the structural basis of enantioselectivity and aid the design of new syntheses.

Experimental Section

General. All chemicals were purchased from Aldrich Chemical Co. (Milwaukee, WI) unless otherwise noted. *N*-Tris(hydroxymethyl)methyl-2-aminoethanesulfonic acid, TES, was purchased from Sigma Chemical Co. (St. Louis, MO). Crude CRL was purchased from Sigma and purified as described previously.[42] Benzene was dried by distillation from calcium hydride under nitrogen. Either the Chem 3D force field (Chem 3D v. 3.0, Cambridge Scientific Computing, Cambridge, MA) or the CVFF force field (Discover and Insight II v.2.0, Biosym Technologies, Inc., San Diego, CA) was used for molecular mechanics calculations.

(±)-Menthyl Pentanoate. A solution of (±)-menthol (0.10 g, 0.64 mmol), pentanoic anhydride (0.16 mL, 0.80 mmol), and 4-(dimethylamino)pyridine (10 mg, 0.08 mmol) in ethyl acetate (10 mL) containing suspended sodium carbonate (85 mg, 0.08 mmol) was stirred at room temperature for 2 h. The reaction mixture was washed with saturated $NaHCO_3$ (10 mL), water (10 mL), and saturated NaCl (10 mL), dried over magnesium sulfate, and concentrated by rotary evaporation to an oil, 0.22 g. Chromatography on a silical gel column (15 cm × 2 cm diameter) eluted with 9:1 hexane–ethyl acetate yielded a pale yellow oil: 0.12 g, 0.50 mmol, 81% yield. R_f = 0.89 (silica gel, 9:1 hexane–ethyl acetate); ^{1}H-NMR ($CDCl_3$, 200 MHz) δ 4.68 (apparent dt, 1, J_1 = 11 Hz, J_2 = 6 Hz, CHOC(O)Bu), 2.29 (t, 2, J = 8 Hz, $C(O)CH_2$), 2.03–0.74 (m, 25); ^{13}C-NMR ($CDCl_3$, 50 MHz) δ 173.3, 73.7, 46.9, 40.9, 34.4, 34.2, 31.3, 27.1, 26.1, 23.3, 22.2, 21.9, 20.7, 16.2, 13.6; MS (Cl/NH_3) m/z (rel intensity) 258 (10, M + NH_4^+), 241 (13, M + H^+), 156 (10), 139 (83), 138 (100), 123 (29).

(1*R*)-Menthyl Hexylphosphonochloridate, 1*R*-Cl. A mixture of diisopropylethylamine (1.25 mL, 7.0 mmol), (1*R*,2*S*,5*R*)-menthol (0.5 g, 3.2 mmol, >98% ee by GC), tetrazole (0.05 g, 0.71 mmol), and hexylphosphonic dichloride (0.55 mL, 3.2 mmol) in dry benzene was stirred at room temperature for 20 h. The solvent was removed under vacuum and the residue was dissolved in hexane–ethyl ether (7:3 mixture, 3 mL). Silica gel column chromatography (15 cm × 2 cm diameter) eluted with 7:3 hexane–ethyl ether afforded a clear oil: 0.18 g, 0.56

(26) Umemura, T.; Hirohara, H. In *Biocatalysis in Agricultural Biotechnology*; Whitaker, J. R., Sonnet, P. E., Eds.; American Chemical Society: Washington, DC, 1989; pp 371–384.
(27) Janssen, A. J. M.; Klunder, A. J. H.; Zwanenburg, B. *Tetrahedron* **1991**, *47*, 7645–7662.
(28) Ziffer, H.; Kawai, K.; Kasai, M.; Imuta, M.; Froussios, C. *J. Org. Chem.* **1983**, *48*, 3017–3021.
(29) Mori, K.; Akao, H. *Tetrahedron* **1980**, *36*, 91–96.
(30) Yamaguchi, Y.; Komatsu, A.; Moore, T. *Nippon Nogei Kagaku Kaishi* **1976**, *50*, 619–620; *Chem. Abstr.* **1976**, *86*, 135481d.
(31) Serreqi, A. N.; Kazlauskas, R. J., unpublished results.
(32) Stamatis, H.; Xenakis, A.; Kolisis, F. N. *Biotechnol. Lett.* **1993**, *15*, 471–476.
(33) Williams, A. C.; Woodley, J. M.; Ellis, P. A.; Narendranathan, T. J.; Lilly, M. D. *Enzyme Microb. Technol.* **1990**, *12*, 260–265.
(34) Brooks, I. K.; Lilly, M. D.; Drozd, J. W. *Enzyme Microb. Technol.* **1986**, *8*, 53–57. Nelboeck-Hochstetter, M.; Seidel, H.; Gauhl, H. Ger. Patent 2 537 339, **1977**; *Chem. Abstr.* **1977**, *86*, 169342z.
(35) Murase, H.; Yoshikawa, K.; Tominaga, Y.; Shimada, Y.; Muro, T.; Shimada, J. Japan Patent 02 299 584, **1990**; *Chem. Abstr.* **1991**, *114*, 141633t.
(36) Yamaguchi, Y.; Komatsu, A.; Moroe, T. *Nippon Nogei Kagaku Kaishi* **1977**, *51*, 411–416; *Chem. Abstr.* **1977**, *87*, 165989p.
(37) Mitsui, Petrochemical Industries, Ltd., Japan Patent 56 015 690, **1981**; *Chem. Abstr.* **1981**, *94*, 207140g.
(38) Schrag, J. D.; Cygler, M.; Winkler, F. K. *J. Biol. Chem.* **1992**, *267*, 4300–4304.
(39) Haas, M. J.; Allen, J.; Berka, T. R. *Gene* **1991**, *109*, 107–113. Yamaguchi, S.; Mase, T.; Takeuchi, K. *Gene* **1991**, *103*, 61–67.
(40) Cygler, M.; Schrag, J. D.; Sussman, J. L.; Harel, M.; Silman, I.; Gentry, M. K.; Doctor, B. P. *Protein Sci.* **1993**, *2*, 366–382.
(41) Gilbert, E. J. *Enzyme Microb. Technol.* **1993**, *15*, 634–645.
(42) Rubin, B.; Jamison, P.; Harrison, D. In *Lipases: Structure, Mechanism and Genetic Engineering*; Alberghina, L., Schmid, R. D., Verger, R., Eds.; VCH: New York, 1991; pp 63–66.

mmol, 18% yield. ^{1}H-NMR (C_6D_6, 200 MHz) δ 4.75–4.38 (m, 1, CHOP), 2.65–0.70 (m, 31); ^{31}P-NMR (C_6D_6, 81 MHz) δ 43.3, 42.5; IR (neat) 2930, 1458, 1267, 1013, 967, 565 cm^{-1}. For mass spectrometry, we prepared the methoxy derivative by adding triethylamine (0.25 mL, 1.8 mmol) and methanol (0.25 mL, 6.2 mmol) to a solution of **1*R*-Cl** (210 mg, 0.64 mmol) in CH_2Cl_2 (2 mL). The reaction mixture was stirred overnight and then concentrated by rotary evaporation. The residue was purified by silica gel column chromatography (10 cm × 1 cm diameter) eluted with 1:1 ethyl ether–petroluem ether affording the methoxy derivative as a clear oil: 150 mg, 0.47 mmol, 74%. MS (Cl/NH_3) m/z (rel intensity) 319 (16, M + H$^+$), 198 (11), 182 (13), 181 (100); exact mass 319.24140 ($C_{17}H_{36}O_3P$ + H requires 319.24019, 3.8 ppm error).

(1*S*)-Menthyl Hexylphosphonochloridate, 1*S*-Cl, was synthesized as described above for the **1*R*** isomer starting with (1*S*,2*R*,5*S*)-menthol (98% ee by GC) affording a clear oil: 0.41 g, 1.27 mmol, 40% yield. ^{1}H-NMR ($CDCl_3$, 200 MHz) δ 4.63–4.45 (m, 1, CHOP), 2.42–0.78 (m, 31); ^{31}P-NMR ($CDCl_3$, 81 MHz) δ 45.0, 44.0; IR (neat) 2930, 1458, 1267, 1078, 540 cm^{-1}. For mass spectrometry, we prepared the methoxy derivative as above. MS (Cl/NH_3) m/z (rel intensity) 319 (16, M + H$^+$), 198 (11), 182 (13), 181 (100); exact mass 319.24170 ($C_{17}H_{36}O_3P$ + H requires 319.24019, 4.7 ppm error).

Enantioselectivity of CRL toward (±)-Menthyl Pentanoate. (±)-Menthyl pentanoate (120 mg, 0.5 mmol) was added to a mixture of toluene (10 mL) and buffer (10 mL, 10 mM phosphate, pH 7.0) containing crude CRL (167 mg). The reaction was stirred rapidly and the pH was maintained at pH 7.0 by automatic addition of NaOH (0.1 N). After 18 h the mixture was extracted with 7:1 ethyl acetate–ethyl ether (4 × 10 mL) and the combined organic extracts were concentrated to an oil. The product menthol and starting ester were separated on a silica gel column (6 cm × 2 cm diameter) eluted with 19:1 petroleum ether–ethyl acetate. The enantiomeric purity of the product menthol (ee_p) was 82% ee (*R*) as measured by capillary gas chromatography on a 30 m Chiraldex G-TA column (AstecTechnologies, Whippany, NJ). Conditions: 1 μL injection, split ratio 100:1, 80 °C, flame ionization detector. The enantiomeric purity of the remaining ester (ee_s), measured in the same manner after cleaving the ester with excess $LiAlH_4$ in tetrahydrofuran, was 23% ee (*S*). The conversion was calculated using $c = ee_s/(ee_s + ee_p)$[18] and the enantiomeric ratio, calculated using $E = \{\ln[(1 - c)(1 - ee_s)]\}/\{\ln[(1 - c)(1 + ee_s)]\}$ or $E = \{\ln[1 - c(1 + ee_p)]\}/\{\ln[1 - c(1 - ee_p)]\}$,[13] was 12.8.

Enzyme Assay. Lipase activity was measured using *p*-nitrophenyl acetate (PNPA) as the substrate. An aliquot (5 μL) of enzyme solution followed by an aliquot of *p*-nitrophenyl acetate (5 μL of a 50 mM solution in acetonitrile) were added to buffer (1.0 mL, 10 mM phosphate, pH 7.5) at 25 °C. The initial rate of formation of *p*-nitrophenolate was monitored at 404 nm for 30 s. An extinction coefficient of 11600 M^{-1} cm^{-1}, which accounts for the incomplete ionization of *p*-nitrophenolate at pH 7.5, was used to calculate activity. Typical activity of purified CRL was 5–10 U/mg of protein where one unit (U) corresponds to 1 μmol of *p*-nitrophenolate released per minute.

Inactivation of CRL by 1*R*-Cl and 1*S*-Cl. To a solution of phosphate buffer (1 mL, 10 mM, pH 7.5) and purified CRL (5 μL of 0.86 g/L in TES buffer, pH 7.4, 14 μM enzyme) was added **1*R*-Cl** (5 μL of a 13 mM solution in acetonitrile). After 16 min, an enzyme assay showed that the hydrolytic activity dropped from 5.5 U/mg to <0.06 U/mg, >98% inactivation. In a similar experiment **1*S*-Cl** also inactivated CRL by >98%.

Crystallographic Analysis of Enzyme-Inactivator Complexes. 1*R*-CRL complex was prepared by dissolving **1*R*-Cl** inactivator in 2-methyl-2,4-pentanediol (4 μL, 30 mM solution) and adding it to an aqueous solution of CRL (20 μL, 0.17 mM solution). Similarly, **1*S*-CRL** complex was prepared by dissolving **1*S*-Cl** inactivator in 2-methyl-2,4-pentanediol (100 mM solution) and adding 1 μL to an aqueous solution of CRL (9 μL, 0.17 mM solution). After 10 min the enzyme showed <2% of the original hydrolytic activity. Crystals of the complexes were grown by vapor diffusion under conditions similar to those used for the unliganded enzyme.[8] The reservoir solution contained 40% (v/v) 2-methyl-2,4-pentanediol, 30 mM sodium acetate buffer, pH 5.3, and 30 mM $CaCl_2$. The complexes were concentrated to 8 mg/mL and crystallization drops contained a 1:1 mixture of the concentrated CRL–inactivator complex solution and reservoir solution. All data were collected on a R-Axis IIC image plate area detector at a crystal-to-detector distance of 110 mm. The X-ray generator was operated at a power of 5 kW (50 kV, 100 mA) and a graphite monochromator was used to isolate the Cu Kα radiation. One crystal was used for collection of a complete data set from each CRL–inactivator complex. Since the crystals were isomorphous to the unliganded "open" form, initial phases for the structural refinement were calculated from the native structure.[8] No solvent molecules were included in the initial model. The inactivator molecules were located in $F_o - F_c$ difference maps. All refinements were done using X-PLOR.[43] Parameters for the inactivator molecule were derived from the structures of model compounds from the Cambridge Structural Database.[44] The inactivator was included in the calculations during the later stages of refinement. Model adjustments were done with FRODO.[45] Table 1 summarizes data collection and refinement statistics.

Acknowledgment. We thank Mrs. Y. Li and Mr. M. Desrochers for technical support and Mr. Tristan Booth for molecular mechanics calculations. R.J.K. thanks NSERC Canada for financial support.

(43) Brünger, A. T. X-PLOR (Version 3.1): A system for X-ray crystallography and NMR; Yale University Press: New Haven, CT, 1992.
(44) Allen, F. H.; Kennard, O.; Taylor, R. *Acc. Chem. Res.* **1983**, *16*, 146–153.
(45) Jones, T. A. *J. Appl. Crystallogr.* **1978**, *11*, 268–272.
(46) Connolly, M. L. *J. Appl. Crystallogr.* **1983**, *16*, 548–558.